Methane Release from Igneous Intrusion of Coal during Late Permian Extinction Events
Author(s): Gregory J. Retallack and A. Hope Jahren
Source: *The Journal of Geology*, Vol. 116, No. 1 (January 2008), pp. 1-20
Published by: The University of Chicago Press
Stable URL: http://www.jstor.org/stable/10.1086/524120
Accessed: 09-01-2017 20:26 UTC

ARTICLES

Methane Release from Igneous Intrusion of Coal during Late Permian Extinction Events

Gregory J. Retallack and A. Hope Jahren[1]

Department of Geological Sciences, University of Oregon, Eugene, Oregon 97403-1272, U.S.A.
(e-mail: gregr@uoregon.edu)

ABSTRACT

Unusually large and locally variable carbon isotope excursions coincident with mass extinctions at the end of the Permian Period (253 Ma) and Guadalupian Epoch (260 Ma) can be attributed to methane outbursts to the atmosphere. Methane has isotopic values ($\delta^{13}C$) low enough to reduce to feasible amounts the carbon required for isotopic mass balance. The duration of the carbon isotopic excursions and inferred methane releases are here constrained to <10,000 yr by counting annual varves in lake deposits and by estimating peat accumulation rates. On paleogeographic maps, the most marked carbon isotope excursions form linear arrays back to plausible methane sources: end-Permian Siberian Traps and Longwood-Bluff intrusions of New Zealand and end-Guadalupian Emeishan Traps of China. Intrusion of coal seams by feeder dikes to flood basalts could create successive thermogenic methane outbursts of the observed timing and magnitude, but these are unreasonably short times for replenishment of marine or permafrost sources of methane. Methane released by fracturing and heating of coal during intrusion of large igneous provinces may have been a planetary hazard comparable with bolide impact.

Online enhancement: tables.

Introduction

The greatest of all known mass extinctions at the Permian-Triassic boundary and another mass extinction at the end of the Guadalupian Epoch (Stanley and Yang 1994) are dated at 252.6 and 260.4 Ma, respectively (Gradstein et al. 2004; Mundil et al. 2004). Both mass extinctions were pronounced disruptions of the global carbon cycle, as indicated by worldwide excursions in isotopic values of carbon in carbonate, bone, and organic matter (Payne et al. 2004; Retallack et al. 2006*a*). Organic carbon isotope values ($\delta^{13}C$) in both marine and nonmarine strata show marked and locally very variable excursions averaging −6.4‰ ± 4.4‰ at 253 Ma (31 examples tabulated by Retallack and Krull [2006]) and −4.0‰ ± 4.1‰ at 260 Ma (10 examples tabulated by Retallack et al. [2006*a*]). Global perturbations of this magnitude on land and in the sea are feasible only with release to the atmosphere of methane because of its unusually low carbon isotopic values (averaging −60‰; Clayton 1998). Mass balance modeling by Berner (2002) shows that the amount of methane needed to explain global isotopic excursions of this magnitude is some 2000 Gt (1 Gt = 10^{15} g), more than current amounts of carbon in all living organisms and soil humus today (Siegenthaler and Sarmiento 1993). Because carbon of volcanoes, air, soils, plants, and most meteorites has much higher isotopic values, the amounts of carbon needed to create such excursions from those sources are larger still, and hence implausible (Retallack and Krull 2006).

Here we examine local variation in end-Permian and end-Guadalupian isotopic excursions on paleogeographic maps as a guide to sources of this isotopically distinct gas. We also reexamine the rapidity of Permian-Triassic isotopic excursions by counting laminations interpreted as annual varves and estimating accumulation rates of coals derived from woody peats through documented carbon iso-

Manuscript received May 29, 2007; accepted October 1, 2007.

[1] Department of Earth and Planetary Sciences, Johns Hopkins University, Baltimore, Maryland 21218, U.S.A.

[The Journal of Geology, 2008, volume 116, p. 1–20] 0022-1376/2008/11601-0001$15.00. DOI: 10.1086/524120

tope excursions in Permian-Triassic boundary sequences of Australia and Antarctica. These data support the idea of methane release to the atmosphere from thermogenic alteration of coal during basaltic intrusion, as recently proposed for marked negative carbon isotope anomalies at 55 (Svensen et al. 2004) and 182 Ma (McElwain et al. 2005; Svensen et al. 2007).

Hints that Late Permian carbon isotope excursions were rapid have come from U/Pb zircon dating at Meishan, China, where two carbon isotope excursions of −4.6‰ (Xu and Yan 1993; Jin et al. 2000) lie between tuffs dated at 251.4 ± 0.3 and 250.7 ± 0.3 Ma (Bowring et al.1998). These two isotopic excursions would have taken about 700 kyr—no more than 1300 kyr and no less than 100 kyr at extremes of dating error (2σ)—and this conclusion is not significantly altered by slightly older (ca. 2-Ma) ages for these samples given by Mundil et al. (2004). Similarly, assumed Milankovitch cycles in the Gartnerkofel core of the Carnic Alps, Austria (Rampino et al. 2000), were used to calculate a rock accumulation rate of 10 cm kyr^{-1}. Using that rate, the most marked carbon isotopic excursion was within 60 kyr. Both Meishan and Gartnerkofel marine carbonate records millennial-scale (kyr) temporal resolution of the carbon isotopic excursion because of mixing of isotopically light bicarbonate with a large reservoir of oceanic bicarbonate before precipitation as carbonate (Berner 2002). A more precise estimate of a comparable isotopic excursion comes from organic carbon in evaporites with annual varves in the Delaware Basin of Texas at the end of the Guadalupian Epoch. In the UNM Phillips 1 core, an isotopic excursion of −2.5‰ $\delta^{13}C_{organic}$ within 5 kyr was followed immediately by an excursion of −3.8‰ $\delta^{13}C_{organic}$ within 10 kyr (Magaritz et al. 1983). This estimate of duration across the Guadalupian-Lopingian boundary, like estimates presented here using comparable varve analysis, is an order of magnitude shorter than U/Pb or wavelet estimates and constrains mechanisms for global Late Permian carbon isotope excursions.

Geological Setting of Samples

Our study sites in Australia and Antarctica are in coal measures that accumulated at high paleolatitudes in large basins between low hills of the Gondwanan interior and an Andean-style volcanic arc (Veevers and Powell 1994). During the Late Permian, Antarctica and Australia were united in the southeastern margin of the Gondwana supercontinent (fig. 1). Periglacial paleosols and other indications of continental ice are older than Late Permian in the Sydney and Transantarctic Basins (Krull 1999; Retallack 1999*a*, 2005*b*), where Late Permian cool temperate, peat swamps were forested by *Glossopteris* and Triassic warm temperate lowlands were forested by *Dicroidium* and *Voltziopsis* (Retallack 1999*b*; Retallack and Krull 1999).

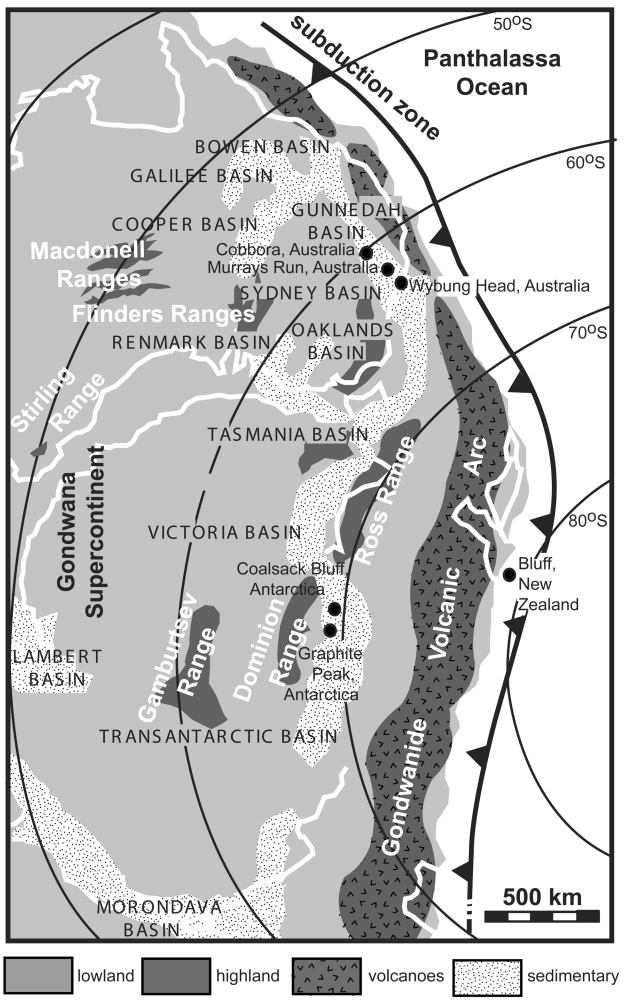

Figure 1. Paleogeographic reconstruction of Australia and Antarctica (after Scotese 1994; Veevers and Powell 1994) showing field sites.

Four specific sites were examined for this study. The Murrays Run bore (33.00067°S, 151.0015°E) is in the northern Sydney Basin, Australia (Morante and Herbert 1994; Morante 1996). Wybung Head (33.19948°S, 151.61901°E) is within Fraser National Park on the north coast of New South Wales (Retallack 1999*b*). Coalsack Bluff (84.23989°S, 162.29979°E) is north of the Beardmore Glacier in the central Transantarctic Mountains (Retallack et al. 2006*b*). Graphite Peak (95.05211°S, 172.36832°E) is south of the Beardmore Glacier in the central

Transantarctic Mountains (Retallack and Krull 1999, 2006).

These four sites were all nonmarine, unlike the stratotype Permian-Triassic boundary marine section near Meishan, China (Jin et al. 2000). Land-sea correlations to establish age of nonmarine sections were difficult until the advent of carbon-isotope chemostratigraphy. Marine sections reveal multiple carbon isotope excursions during the Early Triassic but little change in the Late Permian or early Middle Triassic (Payne et al. 2004), a long-term pattern clear in the nonmarine section at Graphite Peak (fig. 2) and elsewhere (Retallack et al. 2006*a*). A marked sulfur isotope excursion also links marine sections in China and Hungary (Kaiho et al. 2006), with a nonmarine section in South Africa (Maruoka et al. 2003). Additional support for such land-sea correlations comes from independent radiometric dating of nonmarine successions in eastern Australia (Veevers and Powell 1994) and the marine stratotype in China (Bowring et al. 1998; Mundil et al. 2004). Such correlations demonstrate that the mass extinction of marine life at the Permian-Triassic boundary coincided with the mass extinction of the *Glossopteris* flora, which can be recognized on the basis of paleobotany, palynology, and paleosols in both Australia and Antarctica (fig. 2). Chemostratigraphic correlations indicate that *Lystrosaurus* in South Africa straddles the Permian-Triassic boundary, and both *Lystrosaurus* and *Cynognathus* are known from Antarctica (Retallack et al. 2005; Collinson et al. 2006).

The Middle-Late Permian (Guadalupian-Lopingian) boundary 7 m.yr. before the end-Permian (Gradstein et al. 2004; Mundil et al. 2004) also was a time of mass extinction in the sea, comparable in magnitude to end-Cretaceous extinctions (Stanley and Yang 1994). Proposed basal Lopingian stratotype sections near Tieqiao and Penglaitan in south China record a marked negative carbon isotope anomaly (Wang et al. 2004; Kaiho et al. 2005), found in nonmarine sections as well, at Graphite Peak (fig. 2) and elsewhere (Retallack et al. 2006*a*). This boundary coincides with extinction of archaic elements of the *Glossopteris* flora, such as *Gangamopteris cyclopteroides* and *Palaeovittaria kurtzii*, as well as ecosystem-level changes recorded by changes in palynological assemblages and paleosols (fig. 2).

Despite broad similarities between carbon isotope records on land and at sea used for correlation, there are differences important to our interpretations emphasizing nonmarine records. Marine carbonate carbon isotope records are time averaged over millennia and regionally mixed by ocean cur-

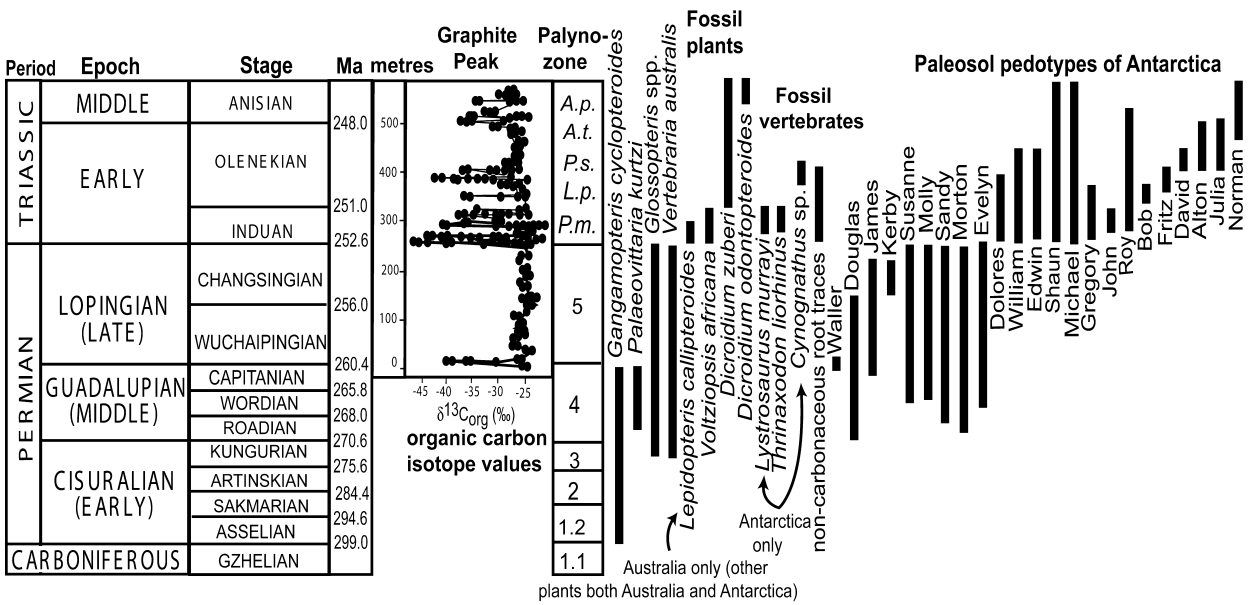

Figure 2. Permian timescale and summary of criteria used for recognition of end-Permian and end-Guadalupian times. Timescale is after Gradstein et al. (2004); Australian palynozones are from Roberts et al. (1996), with abbreviations for (in order) *Protohaplyxypinus microcorpus*, *Lunatisporites pellucidus*, *Protohaploxypinus samoilovichi*, *Aratrisporites tenuispinosus*, and *Aratrisporites parvispinosus* zones. Fossil plant, vertebrate, and pedotype ranges are from Retallack and Krull (1999) and Retallack et al. (2005, 2006*a*).

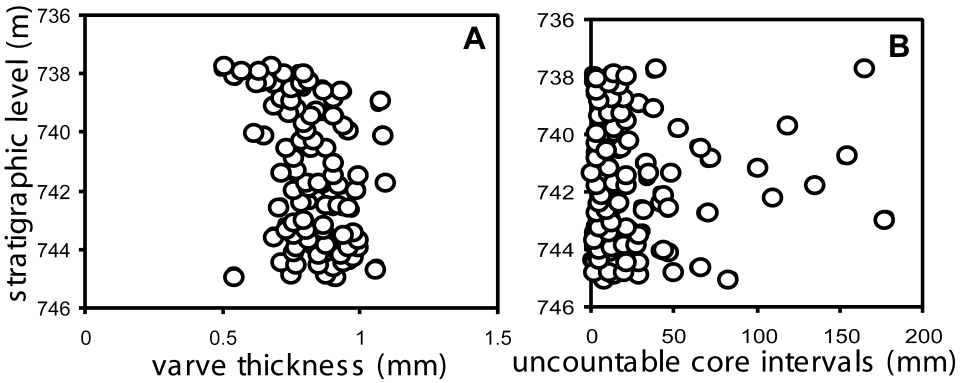

Figure 3. Latest Permian varvelike lamination measurements. Distribution of varve lamination thickness remains relatively constant through 7 m of shale (*A*), as is the thickness of the core (mm) that is uncountable due to fragmentation or destructive sampling (*B*) in latest Permian varved shale of the Murrays Run bore, New South Wales, Australia.

rents, which moderate the exchange of CO_2 with the atmosphere and the diffusion of dissolved bicarbonate from rivers (Siegenthaler and Sarmiento 1993). In contrast, nonmarine organic carbon is a record of annual-decadal variation in atmospheric carbon isotope values assimilated by land plants and incorporated in sediments with leaf shedding and decay (Retallack and Krull 2006). Nonmarine organic carbon values can also reflect changes in photosynthetic pathways, but carbon isotope values of individual Permian and Triassic plants, including succulent lycopsids, indicate that all employed similar C_3 photosynthetic pathways rather than C_4 or CAM metabolism (Retallack and Krull 2006). Open versus closed vegetation canopies can cause minor increases in carbon isotope values (ca. +2‰; Bestland and Krull 1999), and herbaceous vegetation replaced shrubland, forest, and peat swamps for a brief time during the earliest Triassic (Looy 2000). Such a positive shift in carbon isotope value due to open canopy implies that observed negative isotopic excursions were actually more profound than has been observed, so it does not explain magnitude and rapidity of the observed negative excursions.

Methods

Coal seams, laminated shales, and fossil plants were studied petrographically and geochemically to determine whether they formed from woody plants that were seasonally deciduous and so likely to furnish annual records. Varvelike laminations were counted in intact core from the Murrays Run bore, Australia, and they were estimated where core previously had been taken for destructive analysis or had crumbled to fragments in the core trays. Most (82%) of the 5.4-m shaley interval in the Murrays Run core was available for study, and 61% of this was sufficiently intact to allow laminations to be counted. The longest gap of missing core was 47 mm, and the longest segment that was too fragmented for counting was 179 mm (fig. 3*B*). The 3525 laminations counted averaged 0.8 ± 0.1 mm thick (range 0.5–1.1 mm) and were consistent in thickness throughout the counted interval (fig. 3*A*). Average bed thickness compared with overall thickness gave an estimate with two standard deviations of 6750 ± 1350 laminations. A more precise estimate of 6752 laminations comes from interpolation for measured segments of missing or fragmented core from average lamination thickness in intact core immediately below them.

Many of our isotopic data were compiled from prior studies, with paleogeographic analysis using maps of Scotese (1994), and mass balance analysis of atmospheric carbon isotopic values following algorithms of Jahren et al. (2001). Isotopic data from Murrays Run, Graphite Peak, and Coalsack Bluff that were calibrated to the Pee Dee belemnite standard were published previously (Morante and Herbert 1994; Krull and Retallack 2000; Retallack et al. 2006*b*). We also report new carbon isotope analyses, each one averaged from three analyses, of bulk organic residues of HF and HCl maceration, as well as hand-picked cuticles from Wybung Head, Australia (fig. 4). This carbonaceous material was combusted in sealed tubes containing Cu, CuO, and Ag. Released CO_2 was purified and collected for $^{13}C/^{13}C$ measurement relative to Vienna Pee Dee belemnite, using an Isoprime mass spectrometer at Johns Hopkins University. Total organic carbon

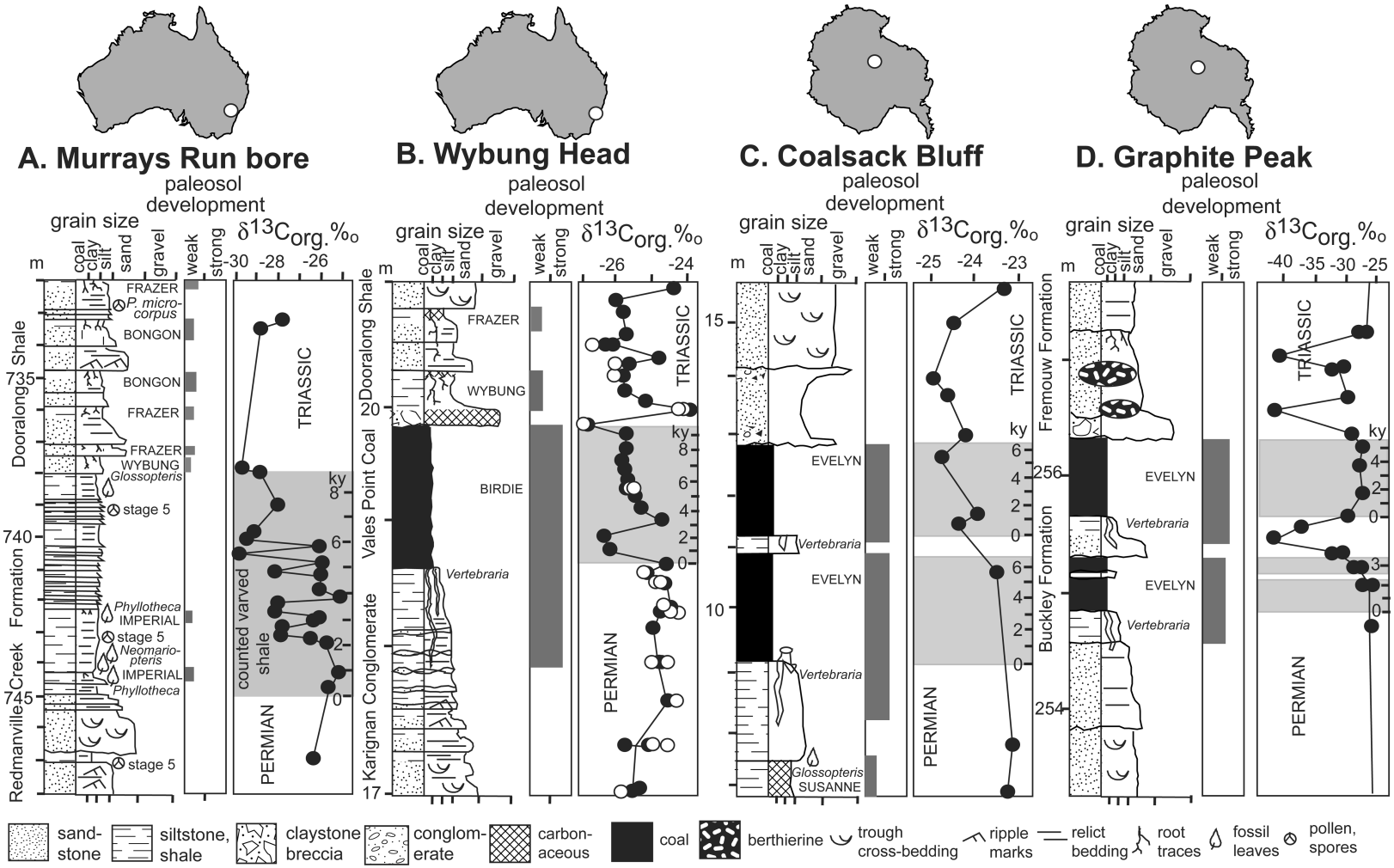

Figure 4. Detailed stratigraphic sections through the Permian-Triassic boundary carbon isotopic excursion in Australia and Antarctica (Retallack 1999*a*; Retallack and Krull 1999; Retallack et al. 2005). Position and degree of development of paleosols are shown as dark gray boxes, following published conventions (Retallack 2001*a*). Open circles for Wybung Head are analyses for hand-picked cuticles; others are for bulk organic carbon of coal and shale (for new isotopic data, see appendix, available in the online edition or from the *Journal of Geology* office). Other isotopic data are from Morante and Herbert (1994), Krull and Retallack (2000), and Retallack et al. (2006*b*).

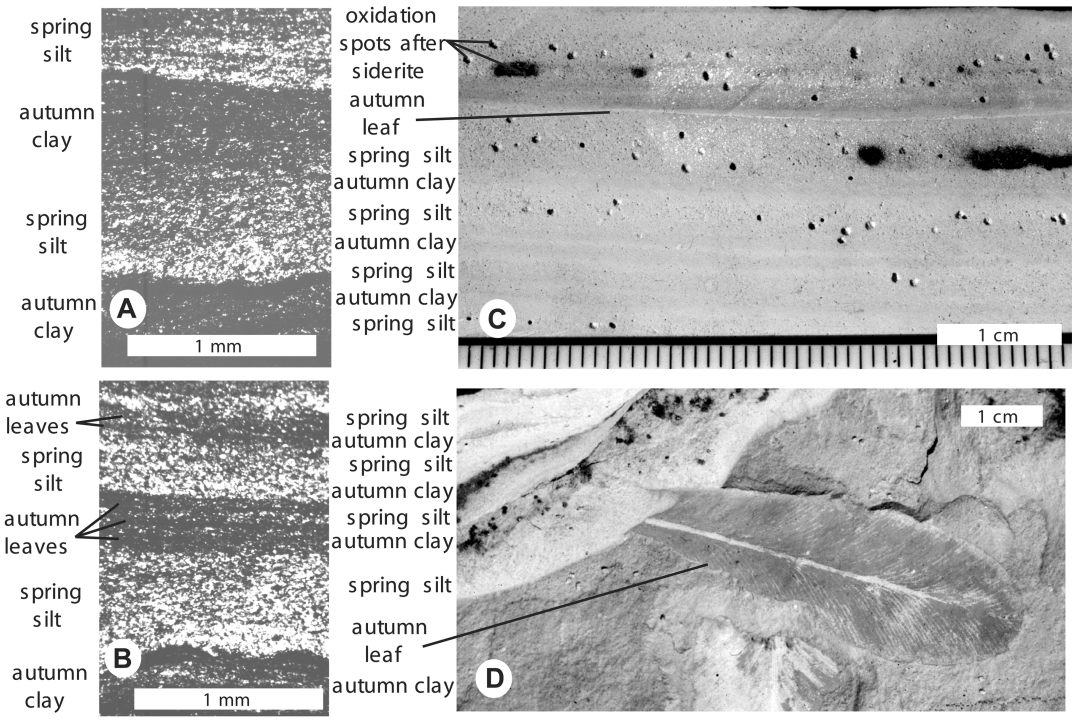

Figure 5. Latest Permian varves and fossil deciduous leaves of *Glossopteris*. *A*, *B*, Photomicrographs of a latest Permian lacustrine varve showing spring thaw siltstone and overlying shale with cross sections of autumnal leaves, from 739.43 m in the Murrays Run bore, New South Wales. *C*, *D*, Polished slab cross section and hand specimen (respectively) of leaves in oxidized varved shales from Cobbora, New South Wales, Australia (Australian Museum specimen F126985). In both cases, rafts of leaves are concentrated below the shaley winter upper portion of the annual varve.

content was also analyzed and did not correlate with $\delta^{13}C$ values, thus ruling out potential errors of carbon isotopic values in organic-lean samples (see appendix, available in the online edition or from the *Journal of Geology* office).

Estimates of Carbon Isotope Excursion Duration

Lamination Analysis. Few paleoenvironmental records have higher resolution than lakes with varves, which are thin (1–3 mm) beds graded in grain size or chemical composition, because each varve represents a single year. Spring thaw and silt influx is followed by summer clay accumulation in a leaf-protected landscape, then late fall and winter freezing of the lake surface (Zillen et al. 2003). Nonannual graded beds can be created by settling of volcanic ash (Zillen et al. 2002) or by multiple annual overturns of chemically and thermally stratified deep lakes (Dickman 1985), but this was not the case for shales of Late Permian lakes in Australia and Antarctica, for reasons outlined next.

Late Permian lacustrine laminae of Australia (fig. 5) and Antarctica (Gunn and Walcott 1962) have erosive bases, indicating complete seasonal overturn of lake water (holomictic) and traction deposition of quartz-rich silts, rather than settling of ash (volcaniclastic) or precipitation of calcite or opal microfossils or crystals (meromictic). Late Permian lakes of Australia and Antarctica were seasonally frozen in a climate with winter snow, judging from associated cold-temperate paleosols (Retallack 1999*a*; Retallack and Krull 1999). Fossil leaves of *Glossopteris* were found only in the upper half of the Late Permian laminations. Leaves are confined to one to four levels within the shaley upper portion of the varve (fig. 5) and are not merely at the top of the normally graded spring silt layer or rolled across bedding planes, as in common in fluvial strata (Retallack et al. 2000). They were not blown ahead of traction currents, settling immediately after silt grains, but they settled with clay in quiet water, in large numbers and in several episodes after silt deposition. Counts of slabs from Cobbora (including fig. 5*D*) show high but variable leaf densities of 680 ± 407 m^{-2} (mean + 1 SD for eight slabs). There is independent paleobiological evidence that *Glossopteris* was seasonally deciduous,

because it had basal petiolar abscission scars as evidence of deliberate leaf shedding and pronounced seasonal growth rings in its wood (Retallack and Dilcher 1988). Our observations support long-standing interpretations that these deposits were annual varves and that *Glossopteris* leaves formed autumnal banks (Gunn and Walcott 1962; Retallack 1980; White 1986).

Annual varves in lacustrine shales of the Murrays Run core, near Wollombi, New South Wales (fig. 4*A*), offer a high-resolution record of end-Permian carbon isotopic excursions within the same sediments (Morante and Herbert 1994). Consistent varve thickness throughout the lacustrine interval (fig. 3*A*) is evidence against large erosional gaps. The Murrays Run core is the most temporally complete Permian-Triassic boundary succession in the Sydney Basin, judging from sequence stratigraphy (Herbert 1995) and preservation of a distinctive basal Triassic paleosol rather than an eroding sandstone paleochannel (Retallack 1999*b*). The unusually high rate of sediment accumulation of these lacustrine beds at a stratigraphic level represented by coal in other parts of the basin was due to contemporaneous downwarping north of the nearby Lochinvar Dome and Hunter-Mooki thrust system (Veevers and Powell 1994). The Murrays Run bore is the only known latest Permian varved shale suitable for this study. Varved shale from the quarry near Cobbora, New South Wales, is a source of commercial landscaping slabs with ferruginized leaves (White 1986), but it has been partly eroded by an Early Triassic paleochannel, and its organic matter was leached by post-Permian deep weathering.

We estimated 6752 annual varves in the Murrays Run bore between the first carbon isotope values significantly lower than average Permian values ($-25.2 \pm 0.7‰$ $\delta^{13}C$; $n = 15$) and the lowest values at final extinction of the *Glossopteris* flora ($-29.7‰$ $\delta^{13}C$) and formation of an earliest Triassic Wybung paleosol (fig. 5*A*). The Murrays Run core shows multiple carbon isotopic excursions through this interval. Individual carbon isotopic excursions each were completed within 800 yr, including two excursions of $-2.2‰$, one of $-2.6‰$, one of $-5.0‰$, and a final excursion of $-4.5‰$. There are two intervening excursions defined by only one high and one low value, but the others noted are all based on duplicate analyses. These are remarkable carbon isotope variations for such short time spans.

Coal Analysis. Further evidence for duration of end-Permian isotopic fluctuations comes from estimates of peat accumulation rate and carbon isotopic records of the last Permian coals at Wybung Head in Australia and Graphite Peak and Coalsack Bluff in the central Transantarctic Mountains (fig. 5*B*–5*D*). Estimates of peat accumulation in Holocene swamp forests are less than 0.5 mm yr^{-1}, because slower rates allow oxygenation and decay. Nor do they subside at rates of >1 mm yr^{-1}, because such rapidly rising stagnant water kills tree roots. Without trees to supply woody debris, the swamp becomes a lake, as in rapidly subsiding Murrays Run lacustrine shales compared to other end-Permian coals (fig. 5). These theoretical constraints of Falini (1965) are confirmed by radiocarbon dating of swamp peats (Retallack 2001*b*). *Sphagnum* moss and other herbaceous plants that form domed peats are not constrained to 0.5–1 mm yr^{-1} subsidence rates (Barber et al. 2003), but their coals are petrographically distinct from vitrinite-rich latest Permian coal of Antarctica and Australia (Diessel 1992). These Late Permian coals were woody peats formed largely from *Glossopteris* tree trunks and compacted to 13% of their original thickness, judging from observations of vitrinite-rich coal petrography and seam splits of the Victoria Tunnel Seam of the Newcastle Coal Measures in New South Wales, Australia (Diessel 1992). This degree of coal compaction is comparable with that of other bituminous coals (Sheldon and Retallack 2001), and it allows computation of peat thickness from coal thickness.

Applying accumulation rate limits and compaction factor to the maximum measured thickness (chosen to accommodate local erosion; Retallack 2005*a*) of Late Permian coals gives 10–19 kyr for duration of peat accumulation at Wybung Head, 10–21 kyr at Coalsack Bluff, and 9–18 kyr at Graphite Peak. The lower ends of these ranges are most likely given suppressed growth and decay rates in high-latitude (65°–85°S) peat swamps (Retallack 1999*b*; Retallack and Krull 1999).

Isotopic analyses of coal might reflect methane generated within the peat or coal, but our analyses of fossil leaf cuticles show carbon isotope values (*open symbols*, fig. 4*B*) similar to those of bulk coal, indicating that the isotopic excursions came from the atmosphere. Similarities in the numbers of excursions in coals at Coalsack Bluff and Graphite Peak (fig. 4*C*, 4*D*), separated by 126 km, also support the idea of atmospheric isotopic signals.

Our isotopic analyses together with estimates for duration of peat accumulation indicate that a carbon isotopic excursion of $-1.9‰$ within the coal at Wybung Head was completed within about 3000 yr, and a later one of $-1.2‰$ was completed within about 2000 yr. The last Permian coal at Graphite Peak was interrupted by shale, soil formation, and then claystone breccia (Retallack 2005*a*), but these

interruptions to peat accumulation were brief, judging from two correlative isotopic excursions 126 km northwest in coal at Coalsack Bluff, each within about 2000 yr. This remarkable isotopic volatility over short times corroborates the latest Permian Murrays Run record (fig. 4*A*).

Paleogeography of Carbon Isotope Excursions

Global compilation of carbon isotope excursions (fig. 6) shows that Late Permian negative carbon isotope excursions were highly variable in magnitude from place to place; see the appendix for a global summary of 55 end-Permian sites and 17 end-Guadalupian sites. Global spacing of these data is not uniform, and large areas remain unknown and uncontoured. Nor are carbonate carbon values (fig. 6, *roman type*) strictly comparable with organic carbon values (fig. 6, *boldface type*), because marine carbonate values are time averaged by oceanic mixing over many millennia, whereas organic carbon on land represents local annual-decadal values (Retallack and Krull 2006). Although the global pattern remains to be established in detail, data density is impressive in tropical islands that later became Europe and China and in the African-Australian-Antarctic portion of Gondwana.

Our new compilation (fig. 6) supports previous observations that the carbon isotope excursions were greater (1) on land than in the sea, (2) in shallow marine than in deep marine environments (Retallack and Krull 2006), and (3) at high than at low paleolatitudes (Krull et al. 2000, 2004; Retallack and Krull 2006). Paleogeographic maps also show that the most profound excursions are neither clumped nor dispersed randomly but form long curved arrays, largely over continental regions. Contouring of the excursions (fig. 6) highlights these curved arrays, which constrain explanations of the carbon isotope excursions.

Explanations for Carbon Isotope Excursions

Three distinct methane sources have been proposed for large amounts of methane necessary to explain Late Permian carbon isotope anomalies: (1) overturn of deep-ocean water, (2) disruption of submarine and permafrost clathrates, and (3) basaltic intrusion of carbonaceous sediments.

Deep-Ocean Water Overturn. Ryskin (2003) proposed that enormous amounts of CH_4 were stored in stagnant deep-ocean water and abruptly released to the atmosphere at the Permian-Triassic boundary. His hypothesis is similar to the proposal that deep oceanic storage of CO_2 (Knoll et al. 1996) or H_2S (Kump et al. 2005) was followed by catastrophic release. These hypotheses require an unusually stratified ocean supplied with CH_4, CO_2, or organic matter by surface-ocean primary production greater than at present, which would be unlikely in the larger-than-modern Late Permian ocean (Hotinski et al. 2001). The CO_2-release model would also create positive carbon isotope excursions in the deep ocean (Hoffman et al.1991), yet deep-ocean Japanese and Canadian terranes have negative excursions (fig. 6). This is not a fatal objection, because deep oceanic carbon is largely derived from surface production, and deep inorganic carbon is unlikely to be buried below the carbonate compensation depth. Another problem for the idea of deep-ocean overturn is the timing of Late Permian deep-marine anoxia, which intensifies rather than declines at the presumed Permian-Triassic boundary release to the atmosphere of chemically reducing gases from the water column (Isozaki 1997; Wignall et al. 1998). More serious objections to the hypothesis of deep-water storage and release of CO_2 and CH_4 are narrow alignment of the most pronounced isotopic anomalies over midcontinental high-latitude regions (fig. 6) rather than predicted extreme marine and coastal isotopic excursions in organic C.

Methane Clathrate Outburst. Dickens et al. (1995) proposed that the end-Paleocene (55 Ma) negative carbon isotope anomaly was created by destabilization of methane bound in ice within permafrost and the pores of submarine sediments. A comparable mechanism has also been suggested for the Permian-Triassic carbon isotope excursion, which is much more negative than the end-Paleocene excursion (Krull et al. 2000, 2004; Berner 2002). Methane is stable in submarine and permafrost clathrates, and abrupt release requires catastrophic destabilization by asteroid impact, volcanic intrusion, or submarine landslide (Retallack and Krull 2006). Mobilization of methane by global warming may also appear geologically abrupt (Benton et al. 2004), though not as abrupt or repetitive as implied by our data (fig. 5).

A serious problem for a clathrate source of Late Permian methane is the modern global inventory of methane clathrates, once thought to be about 10,000 Gt but now reassessed at only 500–2500 Gt (Milkov 2004). If Late Permian clathrate reservoirs were comparable in size, they could not have supplied the amounts of methane needed to explain the isotopic excursions from single reservoirs (Berner 2002; Retallack and Krull 2006).

A more serious objection comes from our documentation here of multiple isotopic excursions within 10 kyr (fig. 5), which is insufficient recharge

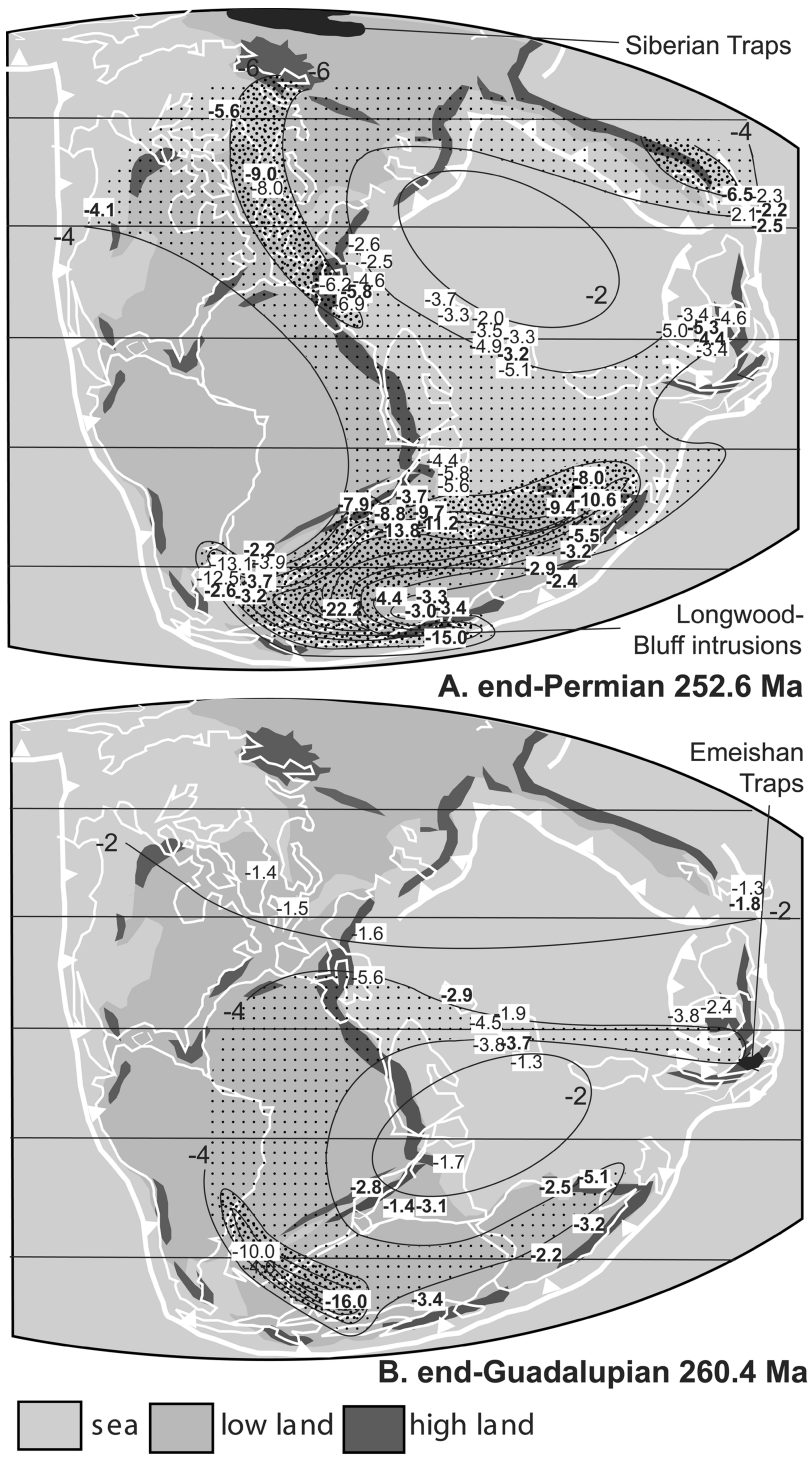

Figure 6. Localities with extreme carbon isotopic excursion (more negative than −6% $\delta^{13}C$) form elongate patterns back to end-Permian Siberian Traps (Kamo et al. 2003) and Longwood-Bluff intrusions of New Zealand (Mortimer et al. 1999) and end-Guadalupian Emeishan Basalt of South China (Zhou et al. 2002). Paleogeographic maps are after Scotese (1994). Carbon excursion values from organic carbon are shown in boldface type, but those from carbonate are in roman type. Intensity of stipple pattern indicates magnitude of the contoured carbon isotopic anomalies. For compilation of isotopic data, see appendix, available in the online edition or from the *Journal of Geology* office.

time for marine clathrate and permafrost reservoirs of required volumes (Berner 2002). The rate of recharge of modern marine clathrate reservoirs, which average 2%–10% of methane per pore volume, is only 1% of methane per pore volume per 10,000 yr (Rempel and Buffet 1998). Modeling of the marine clathrate capacitor from isotopic data for a proposed discharge at the Paleocene-Eocene boundary indicated a recharge time of 200 kyr (Dickins 2001). Submarine and permafrost reservoirs of methane are slow to form because of the low solubility of methane in water and ice of clathrates and the cold, high-pressure conditions of methanogenesis in deep marine sediments. Thus, methane clathrate release cannot explain large, successive Late Permian isotopic excursions on timescales of less than 10 kyr.

Igneous Intrusion of Carbonaceous Sediments. Svensen et al. (2004) proposed an alternative origin of the end-Paleocene (55 Ma) negative carbon isotope excursion by methane release from basaltic intrusion and thermal alteration of carbonaceous North Atlantic marine sediments at the time of the Antrim flood basalts (Storey et al. 2007). McElwain et al. (2005) and Svensen et al. (2007) also suggested this hypothesis for late Early Jurassic (182 Ma; Toarcian) carbon isotopic excursion and methane release coeval with intrusion of Antarctic-African coals by dikes of Ferrar-Drakensburg flood basalts. Subsequent demonstration of 21–40-kyr excursions of $-1.2‰$ $\delta^{13}C_{organic}$ on the longer-term Toarcian excursion of $-5.3‰$ $\delta^{13}C_{organic}$ have been used to argue for methane clathrate releases cued to Milankovitch climatic variation (Kemp et al. 2005). However, these minor releases, also seen before and after the Toarcian excursion, were in addition to more massive atmospheric injections of methane from coal intrusion.

Methane release by coal intrusion as an explanation for Permian-Triassic boundary isotope excursions (Retallack and Krull 2006) satisfies constraints presented here for large amounts of methane mobilized on short timescales (fig. 5) by successive intrusions at point sources largely on land (fig. 6). The timing of outbursts of thermogenic methane is not limited by available gas reservoirs but by local availability of carbonaceous sediments and the timing of intrusions feeding flood basalts, which were rapidly erupted as multiple flows (Wignall 2001). In addition, likely methane sources, modeled amounts, and sinks are promising for the hypothesis of coal intrusion, as outlined next.

Late Permian Sources of Methane from Intruded Coal

The Siberian Traps (figs. 6, 7*A*) were the largest of known flood basalts, and most of the eruptions have been radiometrically dated to the Permian-Triassic boundary (Renne and Basu 1991; Campbell et al. 1992; Czamanske et al. 1998; Reichow et al. 2002). Feeder dikes to the flood basalts have extensively altered Carboniferous and Permian coals of the Tunguska Basin, which includes up to 92 cumulative meters of productive coal (Bogdanova 1971; Strugov 1974; Mazor et al.1979).

Also dated to the Permian-Triassic boundary are intrusions such as the Pourakhino Trondjhemite and Hekeia Gabbro of New Zealand ($^{40}Ar/^{39}Ar$ ages 251.2 ± 0.4 and 249.0 ± 0.4 Ma, respectively; Mortimer et al.1999), which are two of many intrusions extending from Stewart Island to Bluff and the Longwood Range in the South Island (fig. 7*B*). The Bluff-Longwood dikes intruded pyritic black shales with marine molluscs such as *Atomodesma* (Turnbull and Allibone 2003) from the outer continental shelf. Permian marine shales of the Wairaki Hills are also carbonaceous, were altered by comparable intrusions, and yield fossil leaves of *Glossopteris ampla* (Mildenhall 1976). This is a common species in roof shales of the Illawarra and Newcastle Coal Measures of Australia and the Weller Coal Measures of Antarctica, to which New Zealand was attached during the Permian and Triassic (Retallack et al. 2006*a*).

Late Permian volcanics in China include the Emeishan flood basalts, dated to the end of the Guadalupian Epoch by both stratigraphic position between the Maokuo and Wuchaiping Limestones (Xu et al. 2004) and radiometric dating (Zhou et al. 2002; Ali et al. 2005). Eruption of the flood basalts was preceded by regional doming (Xu et al. 2004; He et al. 2006), which created a source terrane in southwestern Yunnan (fig. 7*C*). This terrane had lower relief and was further southwest in the Late Carboniferous (Stephanian), when peat swamps and bauxitic soils covered much of Yunnan, leaving 100 m of coal measures in some places. Early Carboniferous (Tournaisian) coal also is widespread in this region, including one seam 12 m thick (Misch 1946).

Modeled Methane Amounts from Igneous Intrusion of Coal

Past numerical estimates for end-Permian methane outburst have assumed a clathrate methane source

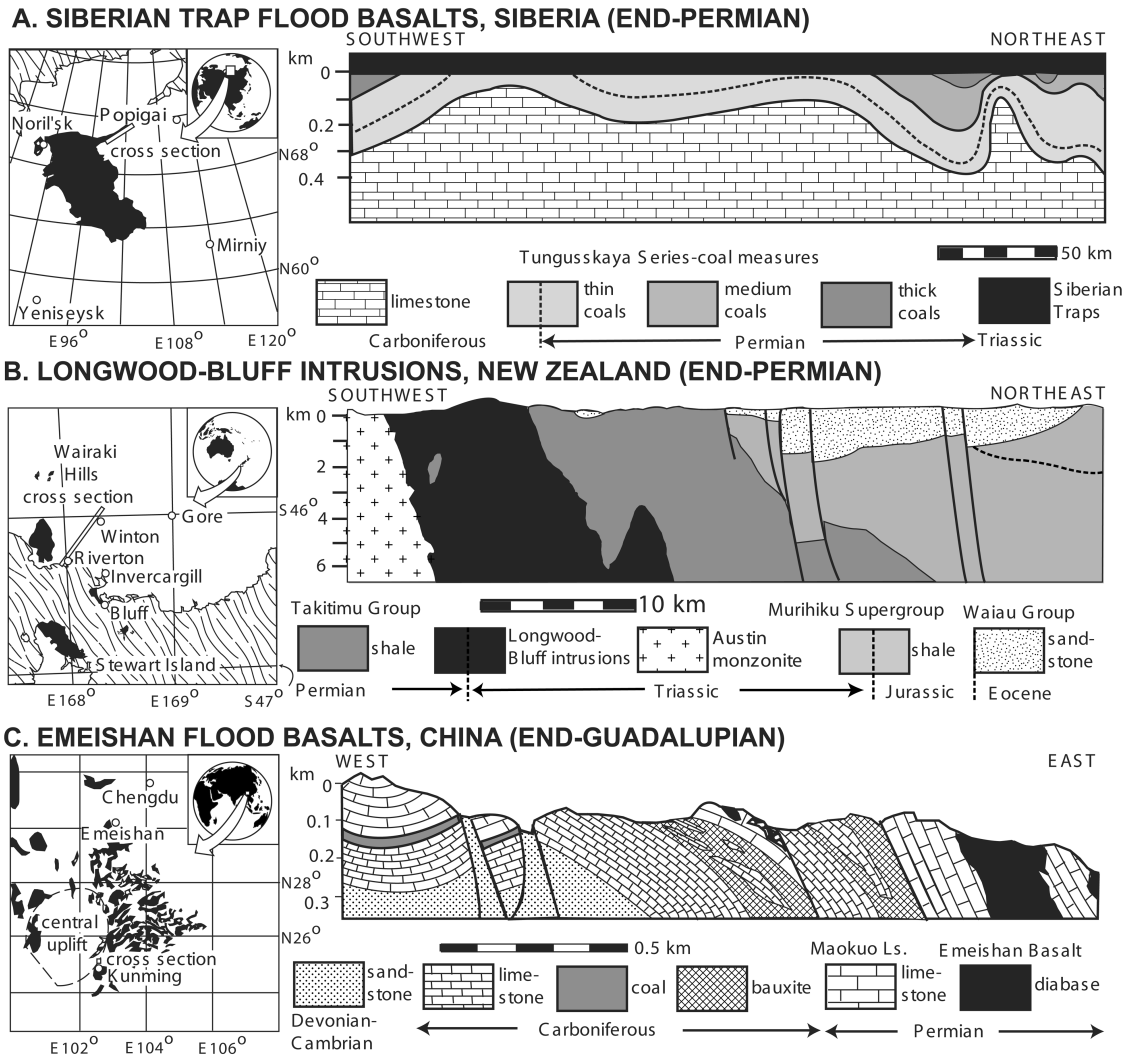

Figure 7. Distributions and cross sections of Late Permian flood basalts and intrusions. *A*, End-Permian Siberian Trap basalts between Norilsk and Popigai, Russia (after Czamanske et al. 1998); *B*, end-Permian Longwood-Bluff intrusions, near Riverton, Bluff and Stewart islands, New Zealand (after Mortimer et al. 1999; Turnbull and Allibone 2003); *C*, Emeishan Basalt and feeder diabase at Liyuantsun, northwest of Kunming, China (after Misch 1946; Xu et al. 2004).

with isotopic composition of −60‰ $\delta^{13}C$ as an average of the known range of −37‰ to −120‰ $\delta^{13}C$ (Krull et al. 2000; Berner 2002). In contrast, thermogenic methane from coal intrusion averages −40‰ $\delta^{13}C$, with a range of −35‰ to −55‰ $\delta^{13}C$ (Clayton 1998). This isotopic difference significantly changes estimates of methane outburst as an explanation for the observed carbon isotopic anomalies, as can be seen by consideration of various carbon emissions associated with large basaltic eruptions (fig. 8). Here we calculate the amount of methane required from each of these sources to explain the average global end-Permian carbon isotopic anomaly of −6.4‰ $\delta^{13}C$ and then evaluate whether these amounts are geologically reasonable.

To calculate methane emission mass, we use an atmospheric mass balance formulation of Jahren et al. (2001):

$$(G_{ap} + G_e) \times \delta_{ac} = G_{ap} \times \delta_{ap} + G_e \times \delta_e. \quad (1)$$

In this equation, G is carbon mass in gigatonnes of carbon, δ is carbon isotope value ($\delta^{13}C$; in ‰), and subscripts are for precrisis (p), crisis (c), atmosphere (a), and emission (e). This formulation does not include effects of the ocean, which reacted to atmo-

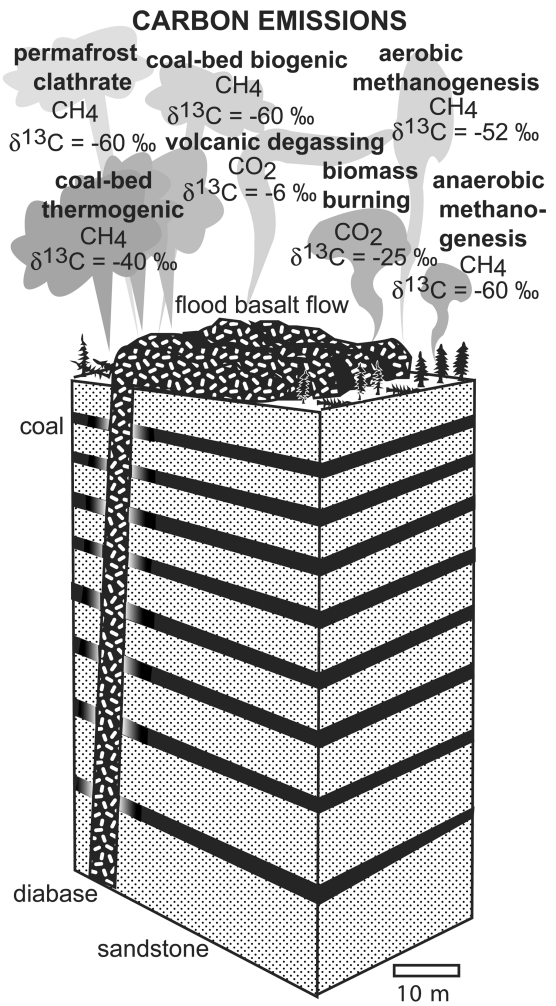

Figure 8. Cartoon for carbon emissions from flood basaltic intrusion of carbonaceous sediments.

spheric change on longer timescales (Retallack and Krull 2006).

To solve for emission volume (G_e) from an assumed emission isotopic value (δ_e), several additional quantities are needed. Isotopic values of Permian and Triassic atmosphere can be calculated from Permian and Triassic isotopic values of organic carbon, using the empirical formulation of Arens et al. (2000) as follows:

$$\delta_a = \frac{(\delta_o + 18.67)}{1.10}. \quad (2)$$

Symbols are as for equation (1) above, but subscript "o" represents organic carbon. The mass of atmospheric carbon both immediately before the crises (G_{ap}) and during the crises (G_{ac}; not needed, but a useful check) can be estimated from CO_2 (in ppm by volume) inferred from stomatal index of seed ferns (Retallack 2001*a*, 2002) calibrated to known CO_2 response of living *Ginkgo* (Wynn 2003). Use of living *Ginkgo* to calibrate extinct seed fern stomatal response is justified by the identical stomatal index of *Lepidopteris* and *Ginkgo* leaves at the Late Triassic localities of Little Switzerland and Upper Umkomaas, South Africa (Retallack 2001*a*). Here we list (table 1) only stomatal index data satisfying rarefaction criteria for reliability: the five-fragment minimum of Royer (2003) and the 500-cell minimum of Retallack (2001*b*).

Estimates of methane emission to the atmosphere required to explain isotopic excursion (table 2) give very large amounts of carbon, and most are geologically unreasonable. For both end-Permian and end-Guadalupian emissions, the amount of carbon needed from biomass exceeds modern amounts of global biomass of 613 Gt (Siegenthaler and Sarmiento 1993), which seems highly unlikely for the Late Permian. No amount of volcanic CO_2 can explain the carbon isotopic anomaly (negative emissions in table 2) because its initial isotopic composition is higher than atmospheric CO_2 (Retallack and Krull 2006; contrary to Payne and Kump 2007). Volcanic CO_2 emissions from lava degassing could create a positive carbon isotope excursion as a return from the isotopic nadir, but that also would require incredible amounts of CO_2 (table 2), much more than the amounts from such enormous eruptions as the Siberian Traps (Wignall 2001).

Biologically created methane produced aerobically by vegetation (Keppler et al. 2006) or anaerobically in coal bed gas (Clayton 1998) or in submarine and permafrost clathrates (Whiticar 2000) has carbon isotopic values of −60‰ to −52‰ $\delta^{13}C$ (average −60‰), low enough to create large isotopic excursions with small amounts. Aerobic methane production at its most optimistic rate of 0.2 Gt yr^{-1} is no more than one-third of the global biogenic production rate of 0.6 Gt yr^{-1} (Keppler et al. 2006), and even that is disputed (Hopkin 2007). Mass extinction of plants (Retallack 1995; Retallack et al. 2006*a*) would decrease rather than increase aerobic methane production. Coal basins have coal bed biogenic and thermogenic methane resources that last for 20–30 yr, but these seldom total more than 1 Gt (Markowski 2001; Montgomery et al. 2001; Higley 2004). With global methane clathrate resources of only 500–2500 Gt (Milkov 2004), hundreds of gigatonnes are unlikely in an individual reservoir. Both coal bed and clathrate methane are very stable in subsurface reservoirs so that rapid release requires geologically unusual conditions of direct extraterrestial bolide impact, igneous intrusion, or

Table 1. Stomatal Index of Fossil Plants and Permian Atmospheric CO_2

Taxon	Locality	Age	Cells	Fragments	Stomatal index	CO_2 (ppmv)	References
Callipteris lepidopteroides	Kosio River, Russia	Mid-Guadalupian	596	5	6.6 ± 1.3	947	Meyen and Migdisova 1969
Lepidopteris martinsii	Aldino, Italy	Early Wuchaipingian	568	14	5.7 ± 1.1	2473	Kerp 1990; Poort and Kerp 1990
Dicroidium nidpurensis	Nidpur, India	Late Wuchaipingian	747	5	7.4 ± .9	551	Bose and Srivastava 1971
Tatarina sp.	Vokma River, Russia	Late Wuchaipingian	1531	7	7.3 ± 1.4	581	Meyen 1969
Tatarina conspicua	Aristovo, Russia	Early Changsingian	2545	10	6.5 ± 1.0	1034	Gomankov and Meyen 1980, 1986
Tatarina pinnnata	Aristovo, Russia	Mid-Changsingian	1387	6	6.2 ± .9	1385	Gomankov and Meyen 1980, 1986
Lepidopteris sp. cf. *L. martinsii*	Sokovka, Russia	Late Changsingian	666	6	5.3 ± 1.1	4264	Naugolnykh 2005
Tatarina antiqua	Nedubrovo, Russia	Induan	1115	5	4.9 ± .4	7876	Krassilov 2003
Lepidopteris callipteroides	Oakdale, Australia	Induan	1748	11	4.9 ± .8	7876	Retallack 2002
Lepidopteris sp.	Tubed, India	Induan	622	5	4.9 ± .9	7876	Bose and Banerji 1976

Note. ppmv = parts per million by volume.
[a] Taxon is comparable to *Lepidopteris martinsii*.

Table 2. End-Permian (252.6 Ma) and End-Guadalupian (260.4 Ma) Methane Release Estimates

Age, CO_2 or CH_4 source	Emission $\delta^{13}C\%$ (δ_e)	Stomatal precrisis CO_2 (ppmv)	Stomatal crisis CO_2 (ppmv)	Stomatal precrisis Gt C (G_{ap})	Atmospheric precrisis $\delta^{13}C\%$ (δ_{ap})	Organic crisis $\delta^{13}C\%$ anomaly ($\delta_{oc} - \delta_{op}$)	Calculated emission Gt C (G_e)	Calculated emission (ppmv)	Calculated crisis CO_2 (ppmv)
251 Ma:									
Thermogenic	−40	1385	7876	2866	−4.85	−6.42	640	1325	2710
Comet	−120	1385	7876	2866	−4.85	−6.42	169	350	1735
Meteorite	−47	1385	7876	2866	−4.85	−6.42	515	1065	2450
Clathrate	−60	1385	7876	2866	−4.85	−6.42	377	781	2166
Coal-bed	−60	1385	7876	2866	−4.85	−6.42	377	781	2166
Aerobic	−52	1385	7876	2866	−4.85	−6.42	452	934	2319
Volcanic	−6	1385	7876	2866	−4.85	−6.42	−3494	−7229	−5844
Biomass	−25	1385	7876	2866	−4.85	−6.42	1339	2771	4156
260.4 Ma:									
Thermogenic	−40	947	2473	1959	−4.85	−3.57	221	458	1405
Comet	−120	947	2473	1959	−4.85	−3.57	63	130	1077
Meteorite	−47	947	2473	1959	−4.85	−3.57	181	375	1322
Clathrate	−60	947	2473	1959	−4.85	−3.57	136	281	1228
Coal-bed	−60	947	2473	1959	−4.85	−3.57	136	281	1228
Aerobic	−52	947	2473	1959	−4.85	−3.57	160	332	1279
Volcanic	−6	947	2473	1959	−4.85	−3.57	−2896	−5991	−5044
Biomass	−25	947	2473	1959	−4.85	−3.57	422	873	1820

Note. Calculations are based on atmospheric mass balance calculations of Jahren et al. (2001), using precrisis and crisis atmospheric CO_2 levels from table 1. ppmv = parts per million by volume.

submarine landslide (Retallack and Krull 2006). Nevertheless, coal bed and clathrate methane could well have contributed to carbon isotope excursions initiated by other causes through feedback processes such as global warming and increased photosynthetic productivity (Berner 2002; Benton et al. 2004).

The possibility that the carbon isotope anomaly was created by meteorite or comet impact remains unlikely, considering links to volcanic intrusions (fig. 6). However, meteorite or comet impact is not impossible (table 2), especially in view of carbonaceous chondrite fragments discovered in Permian-Triassic boundary sediments at Graphite Peak, Antarctica (Basu et al. 2003). The known range of carbon isotope values in chondritic meteorites is −47‰ to +1100‰ $\delta^{13}C$ (Grady et al. 1986; Pillinger 1987), and values of comets and interplanetary dust particles can be as low as −120‰ $\delta^{13}C$ (Jessberger 1999; Messenger 2000). Assuming chondrite carbon content as high as 7 wt% (Vyodkin and Moore 1971), bulk density of 2.2 g cm^{-3} (Wasson 1974), and calculated masses (table 2), impactors capable of creating the observed carbon isotopic anomalies would have been no smaller than 18 km in diameter for the end-Permian chondrites and 13 km for the end-Guadalupian chondrites. Assuming comet carbon content as high as 47 wt% (Thomas et al. 1993) and cometary nucleus bulk density of 0.6 g cm^{-3} (Weissman et al. 2004), a cometary nucleus capable of creating the carbon isotopic anomalies would have to be 10 km in diameter for the end-Permian and 8 km for the end-Guadalupian. A difficulty for both cases is the lack of indisputable craters, which would be as large as or larger (Melosh 1989) than the 150-km end-Cretaceous crater Chicxulub in Yucatan (Turtle et al. 2005). The most likely end-Permian candidate crater (Becker et al. 2004) is disputed regarding geological age, size, and shock-metamorphic minerals (Glikson 2004; Renne et al. 2004; Wignall et al. 2004; Langenhorst et al. 2005). We know of no likely end-Guadalupian crater.

In contrast, thermogenic alteration of coal remains a feasible mechanism for both end-Permian and end-Guadalupian carbon isotope anomalies. At thermogenic production rates of 100–300 L kg^{-1} (Clayton 1998), 4–12 Gt of coal could produce 1 Gt of methane gas. Coals of the Tunguska Basin show contact metamorphism for distances away from intrusions of half the thickness of the end-Permian diabase dikes (Mazor et al. 1979), reducing bulk density from 2.04 to 1.35 g cm^{-3} (Bogdanova 1971). Coal resources in the Tunguska Basin are 92 m in cumulative thickness (Strugov 1974), and earliest Triassic diabase dikes are up to 200 m wide (Mazor et al. 1979; Czamanske et al. 1998). In New Zealand, the end-Permian Pourakhino Trondhjemite is up to 3 km wide and covers 70 km^2 of outcrop (Mortimer et al. 1999), and Late Permian marine rocks are dark gray with organic matter (Mildenhall 1976). In China, diabase feeders of the Emeishan Traps are up to 200 m wide and penetrate up to 100 m of coal measures, including individual seams as thick as 12 m (Misch 1946). A dike 200 m wide by 100 km long could generate 30–90 Gt of methane from the 92 m of proven coal in the Tunguska Basin. Generation of 1000 Gt or so of methane would require thousands of such dikes or extensive sills like those of the Ferrar Dolerites of Antarctica (Marsh 2004). Thermogenic methane generated in this way was efficiently vented to the atmosphere, because coal that is near intrusions is isotopically much more positive than coal farther from intrusions (upper Allan Hills data of Retallack et al. 2006*a*), and cleat-filling carbonate such as dawsonite is so isotopically positive that only magmatic CO_2 remained in alteration zones around intrusions (Golab et al. 2006). Abundant breccia pipes also vented large sills of the Karoo Basin, South Africa (Svensen et al. 2007). Atmospheric redox crises from coal intrusion require intrusion volumes found only in large igneous provinces, which are geologically rare events (Wignall 2001; Courtillot 2002).

Our estimates of thermogenic emissions (table 2) also support the idea of multiple emissions to attain the earliest Triassic and the earliest Late Permian levels of CO_2 seen in stomatal index studies (table 1): at least three successive emissions totaling 2710 Gt for the end-Permian and two emissions totaling 1405 Gt for the end-Guadalupian (table 1). Such a pattern matches the observed records of multiple anomalies at the end-Permian (fig. 4) and end-Guadalupian (Magaritz et al. 1983). Multiple excursions are best revealed by organic carbon isotopic analyses because carbonate carbon isotopic analyses are smoothed and time averaged (Retallack and Krull 2006).

Global Dispersal of Methane from Coal Intrusion

Atmospheric pollution with methane from only a few coal intrusion sources may explain the uneven dispersal of the most profound isotopic excursions (fig. 6). Methane has a residence time in the atmosphere of less than 10 yr before oxidation to CO_2 (Clayton 1998). Isotopically distinctive CO_2 assimilated by plants would be supplied as organic matter to sediment and soil within a few years, and within a year by deciduous plants such as *Glossopteris*.

Other carbon isotopic excursions in pedogenic and marine carbonate also reflect oxidation of atmospheric CH_4 to CO_2 but over millennial timescales of soil formation (Retallack 2001*b*) or ocean mixing (Siegenthaler and Sarmiento 1993). Differences in carbon isotopic values of plants proximal and distal to naturally burning coal indicate that uptake of local CO_2 is much more rapid than atmospheric mixing (Gleason and Kryser 1984). High-CH_4 Atlantic air, distinct from low-CH_4 Arctic air, has been detected at the same station in London within a single day of changing weather (Nisbet 2002). Similarly, preservation of isotopic trends on paleogeographic maps (fig. 6) suggests that some parcels of isotopically distinct gas remained coherent for many days and for considerable distances before completely mixing into the atmosphere and ocean. Nevertheless, much methane would have been mixed globally without early plant uptake and would have contributed to long-term suppression of carbon isotopic values at the end-Guadalupian and end-Permian.

One difference between Late Permian and modern methane in the atmosphere is the large amount of methane modeled from isotopic data (table 2), comparable with large amounts of volcanic ash dispersed by wind from point sources. Volcanic ash from the May 20, 1883, eruption of Mount Krakatau, Indonesia, drifted southwest from the equator on anticyclonic winds, with the intertopical convergence zone in its summer configuration to the north (Simkin and Fiske 1983), similar to the contours in figure 6*B*. Ash from the May 18, 1980, eruption of Mount St. Helens, curved southeast with spring cyclonic midlatitude winds (Sarna-Wojcicki et al. 1981), similar to contours in figure 6*A*.

Late Permian isotopic anomaly alignments (fig. 6) are compatible with Late Permian wind patterns modeled by Gibbs et al. (2002). End-Permian carbon isotope excursions more profound than −6‰ in China, Greenland, Spitsbergen, and Greece form a track consistent with modeled December-January-February wind from the end-Permian Siberian Traps (Renne and Basu 1991; Campbell et al. 1992; Wignall 2001; Kamo et al. 2003). An additional end-Permian track including the Bonaparte Basin of Australia, the Karoo Basin of South Africa, Graphite Peak in Antarctica, and Wairoa Gorge in New Zealand (fig. 6*A*) is consistent with modeled June-July-August winds (Gibbs et al. 2002) from a source in New Zealand, such as end-Permian intrusions near Bluff and Longwood (Mortimer et al. 1999). End-Guadalupian isotopic excursions more profound than −6‰ are found only in the Karoo Basin of South Africa and Graphite Peak in Antarctica (fig. 6*B*), but excursions more profound than −4‰ are known from marine beds of the Bonaparte Basin of Australia, Kaki Vigla in Greece, and Sovetashan in Armenia, and an excursion of −3.8‰ has been reported from Tiequiao, China (Wang et al. 2004). This trend is consistent with modeled December-January-February winds (Gibbs et al. 2002) from a source in the end-Guadalupian Emeishan Basalts of China (Zhou et al. 2002).

Conclusions

Mechanisms of Late Permian mass extinction proposed for methane clathrate outbursts apply equally to a suggested scenario of thermogenic methane outbursts, which also would have depleted atmospheric oxygen. Feedback mechanisms, including volcanic emissions, plant decay, and loss of wetland vegetation, could have amplified the atmospheric redox crisis (Berner 2002), further reducing atmospheric oxygen (Berner et al. 2007). Kill mechanisms during such atmospheric crises include suffocation of marine life by acidosis and hypoxia, plant root mortality by soil water stagnation, and vertebrate death by pulmonary edema (Retallack and Krull 2006). The temporal coincidence between mass extinctions and flood basalt volcanism (Courtillot 2002; Stothers and Rampino 1990) has been dismissed as a coincidence of only a few cases (White and Saunders 2005) or as without adequate causal mechanism for extinction (Wignall 2001). Addition of the end-Guadalupian case to the better-known end-Permian, end-Triassic, and end-Cretaceous cases makes coincidence less likely, and copious generation of methane by intrusion of coals supplies ample killing power. Like meteorite and comet impacts, thermogenic methane outbursts may have been significant hazards to life on Earth.

ACKNOWLEDGMENTS

We thank W. Hagopian for isotopic analyses and N. D. Sheldon, J. G. Wynn, and C. Phillips for discussion. Funded by National Science Foundation grants OPP-0230086 and OPP-0229136. G. J. Retallack contributed fieldwork, and carbon isotopic analyses were obtained in the laboratory of A. H. Jahren.

REFERENCES CITED

Ali, J. R.; Thompson, G. M.; Zhou, M.-F.; and Song, X.-Y. 2005. Emeishan large igneous province, SW China. Lithos 79:475–489.

Arens, N. C.; Jahren, A. H.; and Amundson, R. 2000. Can C_3 plants faithfully record the carbon isotopic composition of atmospheric carbon dioxide? Paleobiology 26:137–164.

Barber, K. E.; Chambers, F. M.; and Maddy, D. 2003. Holocene palaeoclimates from peat stratigraphy: macrofossil proxy climate records from three oceanic raised bogs in England and Ireland. Quat. Sci. Rev. 22:521–539.

Basu, A. R.; Petaev, M. I.; Poreda, R. J.; Jacobsen, S. B.; and Becker, L. 2003. Chondritic meteorite fragments associated with the Permian-Triassic boundary in Antarctica. Science 302:1388–1392.

Becker, L.; Poreda, R. J.; Basu, A. R.; Pope, K. O.; Harrison, T. M.; Nicholson, C.; and Iasky, R. 2004. Bedout: a possible end-Permian impact crater offshore of northwestern Australia. Science 304:1469–1476.

Benton, M. J.; Tverdokhlebov, V. P.; and Surkov, M. V. 2004. Ecosystem remodelling among vertebrates at the Permian-Triassic boundary in Russia. Nature 432: 97–100.

Berner, R. A. 2002. Examination of hypotheses for the Permo-Triassic boundary extinction by carbon cycle modeling. Proc. Natl. Acad. Sci. USA 99:4172–4177.

Berner, R. A.; VandenBrooks, J. M.; and Ward, P. D. 2007. Oxygen and evolution. Science 316:557–558.

Bestland, E. A., and Krull, E.S. 1999. Palaeoenvironment of the early Miocene Kisingiri volcano *Proconsul* sites: evidence from carbon isotopes, palaeosols and hydromagmatic deposits. J. Geol. Soc. Lond. 156:965–976.

Bogdanova, L. A. 1971. Metamorficheskii ryad uglei tungusskogo basseina (Metamorphic grade of coal in the Tunguska Basin). Litol. Polezh. Iskop. 1971:84–98.

Bose, M. N., and Banerji, J. 1976. Some fragmentary plant remains from the Lower Triassic of Auranga Valley, district Palamau. Palaeobotanist 23:139–144.

Bose, M. N., and Srivastava, S. C. 1971. The genus *Dicroidium* from the Triassic of Nidpur, Madhya Pradesh, India. Palaeobotanist 19:41–51.

Bowring, S. B.; Erwin, D. H.; Jin, Y.-G.; Martin, M. W.; Davidek, E. R.; and Wang, W. 1998. U/Pb zircon geochronology and tempo of the end-Permian mass extinction. Science 280:1039–1045.

Campbell, I. H.; Czamanske, G. K.; Fedorenko, V. A.; Hill, R. I.; and Stepanov, V. 1992. Synchronism of the Siberian Traps and the Permian-Triassic boundary. Science 258:1760–1763.

Clayton, J. L. 1998. Geochemistry of coalbed gas: a review. Int. J. Coal Geol. 35:159–173.

Collinson, J. W.; Hammer, W. R.; Askin, R. A.; and Elliot, D. H. 2006. Permian-Triassic boundary in the central Transantarctic Mountains, Antarctica. Geol. Soc. Am. Bull. 118:747–756.

Courtillot, V. 2002. Evolutionary catastrophes: the science of mass extinction. Cambridge, Cambridge University Press, 173 p.

Czamanske, G. K.; Gurevitch, A. B.; Fedorenko, V.; and Simonov, O. 1998. Demise of the Siberian Plume: paleogeographic and paleotectonic reconstruction from the prevolcanic and volcanic record. Int. Geol. Rev. 40:95–115.

Dickens, G. R. 2001. Modeling the global carbon cycle with a gas hydrate capacitor across the latest Paleocene thermal maximum. *In* Paull, C. K., and Dillon, W. P., eds. Natural gas hydrates: occurrence, distribution and detection. Am. Geophys. Union Geophys. Monogr. 124:19–38.

Dickens, G. R.; O'Neil, J. R.; Rea, D. K.; and Owen, R. M. 1995. Dissociation of oceanic methane hydrate as a cause of the carbon isotope excursion at the end of the Paleocene. Paleoceanography 10:965–971.

Dickman, M. D. 1985. Seasonal succession and microlamina formation in a meromictic lake displaying varved sediments. Sedimentology 32:109–118.

Diessel, C. F. K. 1992. Coal-bearing depositional systems. Berlin, Springer, 721 p.

Falini, F. 1965. On the formation of coal deposits of lacustrine origin. Geol. Soc. Am. Bull. 76:1317–1346.

Gibbs, M. T.; Rees, P. M.; Kutzbach, J. E.; Ziegler, A. M.; Behling, P. J.; and Rowley, D. B. 2002. Simulations of Permian climate and comparisons with climate-sensitive sediments. J. Geol. 110:33–55.

Gleason, J. D., and Kryser, T. K. 1984. Stable isotope compositions of gases and vegetation near naturally burning coal. Nature 307:254–257.

Glikson, A. 2004. Comment on "Bedout: a possible end-Permian impact crater offshore of northwestern Australia." Science 306:613.

Golab, A. N.; Carr, P. F.; and Palamara, D. R. 2006. Influence of localised igneous activity on cleat dawsonite formation in Late Permian coal measures, Upper Hunter Valley, Australia. Int. J. Coal Geol. 66:296–304.

Gomankov, A. V., and Meyen, S. V. 1980. On representatives of the family Peltaspermaceae from the Permian of the Russian Platform. Palaeontol. J. 13:240–254.

———. 1986. Tatarinovaya flora (soslav i rasprostranenie v pozdnei permi Evrazi) (Tatarian flora [composition and distribution in the late Permian of Eurasia]). Tr. Akad. Nauk SSSR 401, 174 p.

Gradstein, F. M.; Ogg, J. G.; and Smith, A. G., eds. 2004. A geologic time scale 2004. Cambridge, Cambridge University Press, 589 p.

Grady, M. W.; Wright, J. P.; Carr, L. P.; and Pillinger, C. P. 1986. Compositional differences in enstatite chondrites based on carbon and nitrogen stable isotope

measurements. Geochim. Cosmochim. Acta 50:2799–2813.
Gunn, B. M., and Walcott, R. I. 1962. The geology of the Mt. Markham region, Ross Dependency, Antarctica. N. Z. J. Geol. Geophys. 5:407–426.
He, B.; Xu, Y.-G.; Wang, Y.-M.; and Luo, Z. L. 2006. Sedimentation and lithofacies paleogeography in southwestern China before and after the Emeishan flood volcanism: new insights into surface response to mantle plume activity. J. Geol. 114:117–132.
Herbert, C. 1995. Sequence stratigraphy of the Late Permian coal measures in the Sydney Basin. Aust. J. Earth Sci. 42:391–405.
Higley, D. K. 2004. Undiscovered coalbed methane resources of the Raton Basin, Colorado and New Mexico. Geol. Soc. Am. Abstr. Program 36:83.
Hoffman, A.; Gruszcynski, M.; and Malkowski, K. 1991. On the interrelationship between temporal trends in $\delta^{13}C$, $\delta^{18}O$, and $\delta^{34}S$ in the world ocean. J. Geol. 99: 355–370.
Hopkin, M. 2007. Missing gas saps plant theory. Nature 447:11.
Hotinski, R. M.; Bice, K. L.; Kump, L. R.; Hajjar, R.G.; and Arthur, M. A. 2001. Ocean stagnation and end-Permian anoxia. Geology 29:7–10.
Isozaki, Y. 1997. Permian-Triassic superanoxia and stratified superocean: records from the deep sea. Science 276:235–238.
Jahren, A. H.; Arens, N. C.; Sarmiento, G.; Guerrero, J.; and Amundson, R. 2001. Terrestrial record of methane hydrate dissociation in the Early Cretaceous. Geology 29:159–162.
Jessberger, E. K. 1999. Rocky cometary particulates: their elemental, isotope and mineralogical ingredients. Space Sci. Rev. 90:91–97.
Jin, Y. G.; Wang, Y.; Wang, W.; Shang, Q. H.; Cao, C. Q.; and Erwin, D. H. 2000. Pattern of marine mass extinction near the Permian-Triassic boundary in South China. Science 289:432–436.
Kaiho, K.; Chen, Z.-Q.; Ohashi, T.; Arinobu, T.; Sawada, K.; and Cramer, B. S. 2005. A negative carbon isotope anomaly associated with the earliest Lopingian (Late Permian) mass extinction. Palaeogeogr. Palaeoclimatol. Palaeoecol. 223:172–180.
Kaiho, K.; Kajiwara, Y.; Chen, Z.-Q.; and Gorjan, P. 2006. A sulfur isotope event at the end of the Permian. Chem. Geol. 235:33–47.
Kamo, S. L.; Czamanske, G. K.; Amelin, Y.; Fedorenko, V. A.; Davis, D. W.; and Trofimov, V. R. 2003. Rapid eruption of Siberian flood-volcanic rocks and evidence for coincidence with the Permian-Triassic boundary and mass extinction at 251 Ma. Earth Planet. Sci. Lett. 214:75–91.
Kemp, D. B.; Coe, A. L.; Cohen, A. S.; and Schwark, L. 2005. Astronomical pacing of methane release in the Early Jurassic. Nature 437:396–399.
Keppler, F.; Hamilton, J. T. G.; Braß, M.; and Röckmann, T. 2006. Methane emissions from terrestrial plants under aerobic conditions. Nature 439:187–191.
Kerp, J. H. F. 1990. The study of fossil gymnosperms by means of cuticular analysis. Palaios 5:548–569.
Knoll, A. H.; Bambach, R. K.; Canfield, D. E.; and Grotzinger, J. P. 1996. Comparative earth history and the Late Permian mass extinction. Science 273:452–457.
Krassilov, V. A. 2003. Terrestrial palaeoecology and global change. Moscow, Pensoft, 464 p.
Krull, E. S. 1999. Permian palsa mires as paleoenvironmental proxies. Palaios 14:530–544.
Krull, E. S.; Lehrmann, D. J.; Druke, D.; Kessel, B.; Yu, Y.-Y.; and Li, R.-X. 2004. Stable carbon isotope stratigraphy across the Permian-Triassic boundary in shallow marine platforms, Nanpanjiang Basin, south China. Palaeogeogr. Palaeoclimatol. Palaeoecol. 204: 297–315.
Krull, E. S., and Retallack, G. J. 2000. $\delta^{13}C_{org}$ depth profiles from paleosols across the Permian-Triassic boundary: evidence for methane release. Geol. Soc. Am. Bull. 112:1459–1472.
Krull, E. S.; Retallack, G. J.; Campbell, H. J.; and Lyon, G. L. 2000. $\delta^{13}C_{org}$ chemostratigraphy of the Permian-Triassic boundary in the Maitai Group, New Zealand: evidence for high-latitudinal methane release. N. Z. J. Geol. Geophys. 43:21–32.
Kump, L. R.; Pavlov, A.; and Arthur, M. A. 2005. Massive release of hydrogen sulfide to the surface ocean and atmosphere during intervals of oceanic anoxia. Geology 33:397–400.
Langenhorst, F.; Kyte, F. T.; and Retallack, G. J. 2005. Re-examination of quartz grains from the Permian-Triassic boundary section at Graphite Peak, Antarctica. Proceedings of the 36th Lunar and Planetary Science Conference, abstract 2358.
Looy, C. V. 2000. The Permian-Triassic biotic crisis: collapse and recovery of terrestrial ecosystems. Utrecht, Utrecht University, 113 p.
Magaritz, M.; Anderson, R. Y.; Holser, W. T.; Saltzman, E. S.; and Garber, J. H. 1983. Isotope shifts in the Late Permian of the Delaware Basin, Texas, precisely timed by varved sediments. Earth Planet. Sci. Lett. 66:111–124.
Markowski, A. K. 2001. Coalbed methane resources in Pennsylvania: from old hazard to new energy. Geol. Soc. Am. Abstr. Program 33:74.
Marsh, B. 2004. A magmatic mush column Rosetta Stone: the McMurdo Dry Valleys of Antarctica. EOS: Trans. Am. Geophys. Union 85:497–502.
Maruoka, T.; Koeberl, C.; Hancox, P. J.; and Reimold, W. U. 2003. Sulfur geochemistry across a terrestrial Permian-Triassic boundary section in the Karoo Basin, South Africa. Earth Planet. Sci. Lett. 206:101–117.
Mazor, Y. R.; Piskarev, Y. V.; and Bocharova, L. V. 1979. Characteristics of the accumulation and transformation of coals of the Tunguska Basin. Mosc. Univ. Geol. Bull. 34:28–35.
McElwain, J.; Wade-Murphy, J.; and Hesselbo, S. P. 2005. Changes in carbon dioxide during an oceanic anoxic event linked to intrusion into Gondwana coals. Nature 435:479–482.

Melosh, H. J. 1989. Impact cratering: a geologic process. New York, Oxford University Press, 245 p.

Messenger, S. 2000. Identification of molecular cloud material in interplanetary dust particles. Nature 404: 968–971.

Meyen, S. V. 1969. O rode *Zamiopteris* Schmalhausen i ego sootnoschenii s nekotorimi smezhnaymi rodami (On the genus *Zamiopteris* Schmalhausen and its relationship with other closely related genera). *In* Meyen, S. V., ed. Pteridospermii verkhnego paleozoya i mesozoya (Pteridosperms of the upper Paleozoic and Mesozoic). Tr. Akad. Nauk SSSR 190:85–105.

Meyen, S. V., and Migdisova, A. V. 1969. Epidermalinoe issledovanie angarskikh *Callipteris* i *Compsopteris* (Epidermal investigation of Angaran *Callipteris* and *Compsopteris*). *In* Meyen, S. V., ed. Pteridospermii verkhnego paleozoya i mesozoya (Pteridosperms of the upper Paleozoic and Mesozoic). Tr. Akad. Nauk SSSR 190:59–84.

Mildenhall, D. C. 1976. *Glossopteris ampla* Dana from New Zealand Permian sediments. N. Z. J. Geol. Geophys. 19:130–132.

Milkov, A. V. 2004. Global estimates of hydrate-bound gas in marine sediments: how much is really out there? Earth Sci. Rev. 66:183–197.

Misch, P. 1946. On the facies of the Carboniferous of the Kunming region, eastern Yunnan, with special reference to the bauxite deposits. Geol. Soc. China Bull. 25:1–64.

Montgomery, S. L.; Tabet, D. E.; and Barker, C. E. 2001. Upper Cretaceous Ferron Sandstone: major coalbed methane play in central Utah. Am. Assoc. Petrol. Geol. Bull. 85:199–219.

Morante, R. 1996. Permian and early Triassic isotopic records of carbon and strontium in Australia and a scenario of events about the Permian-Triassic boundary. Hist. Biol. 11:289–310.

Morante, R., and Herbert, C. 1994. Carbon isotope and sequence stratigraphy about the Permian-Triassic boundary in the non-marine Sydney Basin. Proceedings of the 28th Newcastle Symposium, Advances in the Study of the Sydney Basin 28:102–109.

Mortimer, N.; Gans, P.; Calvert, A.; and Walker, N. 1999. Geology and thermochronometry of the east edge of the Median Batholith (Median Tectonic Zone): a new perspective on Permian to Cretaceous crustal growth of New Zealand. Island Arc 8:404–425.

Mundil, R.; Ludwig, K. R.; Metcalfe, I.; and Renne, P. R. 2004. Age and timing of the Permian mass extinctions: U/Pb dating of closed-system zircons. Science 305:1760–1763.

Naugolnykh, S. V. 2005. Upper Permian flora of Vjazniki (European part of Russia), its Zechstein appearance and the nature of the Permian/Triassic extinction. *In* Lucas, S. G., and Ziegler, K. E., eds. The nonmarine Permian. N. M. Mus. Nat. Hist. Sci. Bull. 30:226–242.

Nisbet, E. G. 2002. Have sudden large releases of methane from geological reservoirs occurred since the Late Glacial Maximum, and could such releases occur again? Philos. Trans. R. Soc. A 360:581–607.

Payne, J. L., and Kump, L. R. 2007. Evidence for recurrent Early Triassic massive volcanism from quantitative interpretation of carbon isotope fluctuation. Earth Planet. Sci. Lett. 256:264–277.

Payne, J. L.; Lehrmann, D. J.; Wei, J. Y.; Orchard, M. J.; Schrag, D. P.; and Knoll, A. H. 2004. Large perturbations of the carbon cycle during recovery from the end-Permian extinction. Science 305:506–509.

Pillinger, C. Y. 1987. Stable isotope measurements of meteorites and cosmic dust grains. Philos. Trans. R. Soc. A 323:313–322.

Poort, R. J., and Kerp, J. H. F. 1990. Aspects of Permian palaeobotany and palynology. XI. On the recognition of true peltasperms in the Upper Permian of western and central Europe and a reclassification of species formerly included in *Peltaspermum* Harris. Rev. Palaeobot. Palynol. 63:197–225.

Rampino, M. R.; Prokoph, A.; and Adler, A. 2000. Tempo of the end-Permian event: high-resolution cyclostratigraphy at the Permian-Triassic boundary. Geology 28:643–646.

Reichow, M. K.; Saunders, A. D.; White, R. V.; Pringle, M. S.; Al'Mukhamedov, A. I.; Medvedev, A. I.; and Kirda, N. P. 2002. $^{40}Ar/^{39}Ar$ dates from the West Siberian Basin: Siberian flood basalt province doubled. Science 296:1846–1849.

Rempel, A. W., and Buffet, B. A. 1998. Mathematical models of gas hydrate accumulation. *In* Henriet, J. P., and Mienert, J., eds. Gas hydrates: relevance to world margin stability and climate change. Geol. Soc. Lond. Spec. Publ. 137:63–74.

Renne, P. R., and Basu, A. R. 1991. Rapid eruption of the Siberian Traps flood basalts at the Permo-Triassic boundary. Science 253:176–179.

Renne, P. R.; Melosh, H. J.; Farley, K. A.; Riemold, W. U.; Koeberl, C.; Kelly, S. P.; and Ivanov, B. Q. 2004. Is Bedout an impact crater? take 2. Science 306:610–611.

Retallack, G. J. 1980. Late Carboniferous to Middle Triassic megafossil floras from the Sydney Basin. *In* Herbert, C., and Helby, R., eds. A guide to the Sydney Basin. Geol. Surv. N. S. W. Bull. 26:385–430.

———. 1995. Permian-Triassic life crisis on land. Science 266:77–80.

———. 1999*a*. Permafrost palaeoclimate of Permian palaeosols in the Gerringong volcanic facies of New South Wales. Aust. J. Earth Sci. 46:11–22.

———. 1999*b*. Post-apocalyptic greenhouse paleoclimate revealed by earliest Triassic paleosols in the Sydney Basin, Australia. Geol. Soc. Am. Bull. 111:52–70.

———. 2001*a*. A 300-million-year record of atmospheric carbon dioxide from fossil plant cuticles. Nature 411: 287–290.

———. 2001*b*. Soils of the past. Oxford, Blackwell, 404 p.

———. 2002. *Lepidopteris callipteroides*, an earliest Triassic seed fern of the Sydney Basin, southeastern Australia. Alcheringa 26:475–500.

———. 2005*a*. Earliest Triassic claystone breccias and soil erosion crisis. J. Sediment. Res. 75:663–679.

———. 2005*b*. Permian greenhouse crises. *In* Lucas, S.

G., and Zeigler, K. E., eds, The nonmarine Permian. N. M. Mus. Nat. Hist. Sci. Bull. 30:256–269.
Retallack, G. J.; Bestland, E. A.; and Fremd, T. J. 2000. Eocene and Oligocene paleosols of central Oregon. Geol. Soc. Am. Spec. Pap. 344, 192 p.
Retallack, G. J., and Dilcher, D. L. 1988. Reconstructions of selected seed ferns. Ann. Mo. Bot. Gard. 75:1010–1057.
Retallack, G. J.; Greaver, T.; and Jahren, A. H. 2006*b*. Return to Coalsack Bluff and the Permian-Triassic boundary in Antarctica. Global Planet. Change 55:90–108.
Retallack, G. J.; Jahren, A. H.; Sheldon, N. D.; Chakrabarti, R.; Metzger, C. A.; and Smith, R. M. H. 2005. Permian-Triassic boundary in Antarctica. Antarct. Sci. 17:241–258.
Retallack, G. J., and Krull, E. S. 1999. Landscape ecological shift at the Permian-Triassic boundary in Antarctica. Aust. J. Earth Sci. 46:785–812.
———. 2006. Carbon isotopic evidence for terminal-Permian methane outbursts and their role in extinctions of animals, plants, coral reefs and peat swamps. *In* Greb, S., and DiMichele, W. A., eds. Wetlands through time. Geol. Soc. Am. Spec. Pap. 399:249–268.
Retallack, G. J.; Metzger, C. A.; Greaver, T.; Jahren, A. H.; Smith, R. M. H.; and Sheldon, N. D. 2006*a*. Middle-Late Permian mass extinction on land. Geol. Soc. Am. Bull. 118:1398–1411.
Roberts, J.; Claoué-Long, J. C.; and Foster, C. B. 1996. SHRIMP zircon dating of the Permian System of eastern Australia. Aust. J. Earth Sci. 43:401–421.
Royer, D. L. 2003. Estimating latest Cretaceous and Tertiary atmospheric CO_2 from stomatal indices. *In* Wing, S. L.; Gingerich, P. D.; Schmitz, B.; and Thomas, E., eds. Causes and consequences of globally warm climates in the early Paleogene. Geol. Soc. Am. Spec. Pap. 369:79–93.
Ryskin, G. 2003. Methane-driven oceanic eruptions and mass extinctions. Geology 31:741–744.
Sarna-Wojcicki, A. M.; Waitt, R. B.; Woodward, M. J.; Shipley, S.; and Rivera, J. 1981. Premagmatic ash erupted from March 27 through May 14, 1980—extent, mass, volume and composition. *In* Lipman, P. W., and Mulineaux, D. R., eds. The 1980 eruption of Mount St. Helens, Washington. U.S. Geol. Surv. Prof. Pap. 1250:577–600.
Scotese, C. R. 1994. Paleogeographic map. *In* Klein, G. D., ed. Pangea: paleoclimate, tectonics and sedimentation during accretion, zenith, and breakup of a supercontinent. Geol. Soc. Am. Spec. Pap. 288:7.
Sheldon, N. D., and Retallack, G. J. 2001. Equation for compaction of paleosols due to burial. Geology 29: 247–250.
Siegenthaler, U., and Sarmiento, J. L. 1993. Atmospheric carbon dioxide and the ocean. Nature 365:119–125.
Simkin, T., and Fiske, R. S. 1983. Krakatau 1883. Washington, DC, Smithsonian Institution, 464 p.
Stanley, S. M., and Yang, X. 1994. A double mass extinction at the end of the Paleozoic era. Science 266: 1340–1344.
Storey, M.; Duncan, R. A.; and Swisher, C. C. 2007. Paleocene-Eocene thermal maximum and opening of the northeast Atlantic. Science 316:587–589.
Stothers, R. B., and Rampino, M. R. 1990. Periodicity in flood basalts, mass extinctions and impacts: a statistical view and a model. *In* Sharpton, V. R., and Ward, P. E., eds. Global catastrophes in Earth history. Geol. Soc. Am. Spec. Pap. 247:9–17.
Strugov, A. S. 1974. A comparative geologic characterization of the coal basins on the Siberian Platform. Sov. Geol. Geophys. 15:3–15.
Svensen, H.; Planke, S.; Chevallier, L.; Malthe-Sørenssen, A.; Corfu, F.; and Jamtveit, B. 2004. Hydrothermal venting of greenhouse gases triggering Early Jurassic global warming. Earth Planet. Sci. Lett. 256:554–566.
Svensen, H.; Planke, S.; Malthe-Sørenssen, A.; Jamtveit, B.; Myklebust, R.; Rasmussen, E.; Torfinn, R.; and Rey, S. S. 2007. Release of methane from a volcanic basin as a mechanism for initial Eocene global warming. Nature 429:542–545.
Thomas, K.; Blanford, G. E.; Keller, L. P.; Flock, W.; and McKay, D. S. 1993. Carbon abundance and silicate mineralogy of anhydrous interplanetary dust particles. Geochim. Cosmochim. Acta 51:1551–1566.
Turnbull, I. M., and Allibone, A. H. 2003. Geology of the Murihiku area. Institute of Geological and Nuclear Sciences map, scale 1 : 250,000. Lower Hutt, New Zealand Institute of Geological and Nuclear Sciences, 74 p.
Turtle, E. P.; Pierazzo, E.; Collins, G. S.; Osinski, G. R.; Melosh, H. J.; Morgan, J. V.; and Reimold, W. U. 2005. Impact structures: what does crater diameter mean? *In* Kenkmann, T.; Hörz, F.; and Deutsch, A., eds. Large impact craters. III. Geol. Soc. Am. Spec. Pap. 384:1–24.
Veevers, J. J., and Powell, C. M., eds. 1994. Permian-Triassic Pangean basins and foldbelts along the Panthalassan margin of Gondwanaland. Geol. Soc. Am. Mem. 184, 368 p.
Vyodkin, G. P., and Moore, C. B. 1971. Carbon. *In* Wasson, B., ed. Handbook of elemental abundance of meteorities. New York, Gordon and Breach, p. 81–91.
Wang, W.; Cao, C-Q.; and Wang, Y. 2004. The carbon isotope excursion on GSSP candidate section of Lopingian-Guadalupian boundary. Earth Planet. Sci. Lett. 220: 57–67.
Wasson, J. T. 1974. Meteorites: classification and properties. Berlin, Springer, 316 p.
Weissman, P. R.; Asphaug, E.; and Lowry, S. C. 2004. Structure and density of cometary nuclei. *In* Festaou, M. C.; Keller, H. V.; and Weaver, H. A., eds. Comets II. Tucson, University of Arizona Press, p. 337–357.
White, M. E. 1986. The greening of Gondwana. Balgowlah, Australia, Reed, 256 p.
White, R. V., and Saunders, A. D. 2005. Volcanisms, impact and mass extinction: credible or incredible coincidences? Lithos 79:299–316.
Whiticar, M. J. 2000. Can stable isotopes and global budgets be used to constrain atmospheric methane bud-

gets? *In* Khalil, M. A. K., ed. Atmospheric methane. Berlin, Springer, p. 63–85.

Wignall, P. B. 2001. Large igneous provinces and mass extinctions. Earth Sci. Rev. 53:1–33.

Wignall, P. B.; Morante, R.; and Newton, R. 1998. The Permo-Triassic transition in Spitzbergen: $\delta^{13}C_{org}$ chemostratigraphy, Fe and S geochemistry, facies, fauna and trace fossils. Geol. Mag. 135:47–62.

Wignall, P. B.; Thomas, B.; Willink, R.; and Watling, J. 2004. Is Bedout an impact crater? take 1. Science 306: 609.

Wynn, J. G. 2003. Towards a physically based model of CO_2-induced stomatal frequency response. New Phytol. 157:391–398.

Xu, D. Y., and Yan, Z. 1993. Carbon isotopes and iridium event markers near Permian-Triassic boundary in the Meishan section, Zhejiang. Palaeogeogr. Palaeoclimatol. Palaeoecol. 104:171–175.

Xu, Y.-G.; He, B.; Chung, S.-L.; Menzies, M. A.; and Frey, F. A. 2004. Geologic, geochemical, and geophysical consequences of plume involvement in the Emeishan flood-basalt province. Geology 32:917–920.

Zhou, M.; Malpas, J.; Song, X.-Y.; Robinson, P. T.; Min, S.; Kennedy, A. K.; Lesher, C. M.; and Keays, R. R. 2002. A temporal link between the Emeishan large igneous province (SW China) and the end-Guadalupian mass extinction. Earth Planet. Sci. Lett. 196:113–122.

Zillen, L. M.; Snowball, I. F; Sandgren, P.; and Stanton, T. 2003. Occurrence of varved lake sediment sequences in Vamtland, west central Sweden: lake characteristics, varve chronology and AMS radiocarbon dating. Boreas 32:612–626.

Zillen, L. M.; Wastegård, S.; and Snowball, I. F. 2002. Calendar year ages of three mid-Holocene tephra layers in varved sediments in west central Sweden. Quat. Sci. Rev. 21:1583–1591.